

Damping of de Haas-van Alphen oscillations and vortex-lattice disorder in the peak-effect region of extreme type-II borocarbide superconductors

A. Maniv,¹ T. Maniv,^{2,*} V. Zhuravlev,² B. Bergk,³ J. Wosnitzer,³ A. Köhler,⁴ G. Behr,⁴ P. C. Canfield,⁵ and J. E. Sonier^{6,7}

¹*NRCN, PO Box 9001, Beer Sheva, IL-84190, Israel*

²*Schulich Faculty of Chemistry, Technion-Israel Institute of Technology, Haifa IL-32000, Israel*

³*Hochfeld-Magnetlabor Dresden (HLD), Helmholtz-Zentrum Dresden-Rossendorf, DE-01314 Dresden, Germany*

⁴*Leibniz-Institut für Festkörper- und Werkstoffforschung Dresden, DE-01171 Dresden, Germany*

⁵*Ames Laboratory and Department of Physics, Iowa State University, Ames, Iowa 50011, USA*

⁶*Department of Physics, Simon Fraser University, Burnaby, British Columbia, Canada V6T 1Z1*

⁷*Canadian Institute for Advanced Research, Toronto, Ontario, Canada*

(Received 8 December 2010; revised manuscript received 27 January 2011; published 14 March 2011)

The study of magnetic quantum oscillations in the superconducting state is of fundamental importance for understanding the nature of superconductivity under high magnetic fields. However, although studied for more than three decades, this phenomenon poses several basic questions that still defy satisfactory answers. A key controversial issue concerns the additional damping observed in the vortex state of many strong type-II superconductors. Here, we show results of μ SR, dHvA, and superconducting quantum interference device magnetization measurements on borocarbide superconductors, initially aimed at investigating the “phase-smearing” effect due to inhomogeneous field broadening. It is found, however, that a sharp drop observed in the dHvA amplitude just below H_{c2} is correlated with enhanced disorder of the vortex lattice in the peak-effect region, where the phase-smearing effect is negligible. It is concluded that quasiparticle scattering by the pair potential is significantly enhanced due to vortex-lattice disorder, thus generating additional damping in the dHvA amplitude.

DOI: [10.1103/PhysRevB.83.104505](https://doi.org/10.1103/PhysRevB.83.104505)

PACS number(s): 74.25.Ha, 74.25.Uv, 74.70.Dd

I. INTRODUCTION

Revealing the mechanism in which a clean, ordered superconducting (SC) material at very low temperatures responds to the application of an external magnetic field is of crucial importance for understanding the phenomenon of superconductivity at its most fundamental level. Surprisingly, as compared to high-field superconductivity under “nonideal” conditions, i.e., in dirty or disordered materials at relatively high temperatures, the “ideal” SC states at low temperatures under high magnetic fields are currently not well understood. In particular, the form of the ground SC state, even for a conventional superconductor, under conditions of Landau quantization of the underlying normal electron states is currently unknown.¹ The need for such a theory has been greatly intensified recently due to the striking observations of Shubnikov–de Haas and dHvA oscillations in high-temperature copper-oxide superconductors.² Since the experimental data accumulated so far in the SC state of the latter compounds are quite limited and not very informative, and the microscopic mechanism underlying their SC states has yet to be revealed, our focus in this paper is on more conventional strong type-II superconductors, which were extensively investigated by the dHvA effect.³

The intriguing situation involved in developing a theory for quantum magnetic oscillations (QMO) in the SC state may be illustrated by the extensive investigations performed on the nonmagnetic borocarbide superconductors $\text{YNi}_2\text{B}_2\text{C}$, and $\text{LuNi}_2\text{B}_2\text{C}$.^{4–7} Terashima *et al.*⁴ applied the field-modulation technique to $\text{YNi}_2\text{B}_2\text{C}$, finding a strong suppression of the dHvA amplitude just below the entrance to the SC state, followed by a recovery of the signal at slightly lower fields and a very smooth additional damping over a large field range below the SC transition. The small region of strong additional

damping was found to correlate with that of a significant peak observed in the measured magnetization (the so-called peak effect, PE). Remarkable persistence of the dHvA signal deep in the vortex state of $\text{LuNi}_2\text{B}_2\text{C}$ has also been reported by Isshiki *et al.*⁵

Similarly, large additional damping of the dHvA signal, coinciding with the onset of the PE, was recently observed in $\text{YNi}_2\text{B}_2\text{C}$ by employing the cantilever torque technique,⁶ with the signal persisting at significantly lower fields (down to 3 T). Finally, in a series of dHvA measurements carried out very recently on $\text{LuNi}_2\text{B}_2\text{C}$ by the field-modulation technique,⁷ the salient features reported for $\text{YNi}_2\text{B}_2\text{C}$ (Refs. 4 and 6) have been essentially confirmed (Fig. 1). Note that indications of similar features of the additional damping in the SC state could be seen in dHvA data of other materials (e.g., in V_3Si , see Refs. 1 and 8); however, the PE region has not been examined in these studies.

The current theoretical approaches to the phenomena of QMO in the vortex state¹ do not provide a consistent predictive framework for a quantitative interpretation of the intriguing experimental results. The mean-field theories based on a detailed exposition of the quasiparticle excitations obtained by solving the corresponding Bogoliubov–de Gennes equations for an ordered vortex lattice^{9–11} provide insight into fine features of the Landau band structure, but lose their transparency very quickly and become heavily numerical at early stages of their application to any observable quantity. A simple formula for the additional damping,^{12,13} used frequently in the literature, has been shown to be essentially valid only in the limiting case of a random vortex distribution.¹ The resulting additional damping rate of QMO seriously overestimates the rate calculated numerically (see Fig. 8 in Ref. 11) for an Abrikosov vortex lattice.

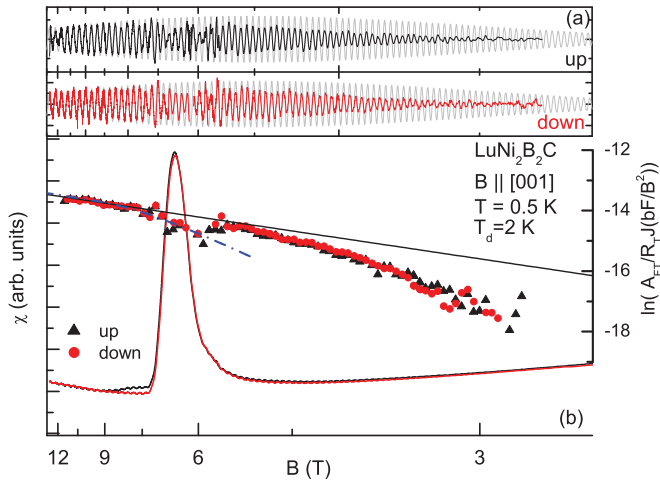


FIG. 1. (Color online) (a) dHvA oscillation signals for upward and downward field sweeps, respectively, measured on $\text{LuNi}_2\text{B}_2\text{C}$ after background subtraction, and (b) the corresponding Dingle plots (triangles and circles, respectively). The gray oscillatory lines in (a) represent the extrapolated dHvA signal, based on the normal-state Lifshitz-Kosevich formula, whereas the solid straight line in (b) is the corresponding Dingle plot. The total magnetization for both field sweeps (solid curves) is also shown in (b). The dashed-dotted line in (b) represents the result of a calculation based on the random vortex distribution model with the zero-field order parameter $\Delta_0 = 4$ meV and mean field $H_{c2} = 8$ T. Measurements were done at 0.5 K.

This may indicate that enhanced quasiparticle scattering by the SC pair potential due to strong disorder of the vortex lattice in the PE region is responsible for the enhanced additional damping reported in Refs. 4, 6, and 7. However, as proposed in Ref. 4, an increased phase-smearing effect, i.e., broadening of Landau levels by the inhomogeneity of the internal magnetic field associated with displaced flux lines by random pinning centers, might also be responsible for the enhanced damping in the PE region.

To gain deeper insight into the origin of the additional damping of the dHvA oscillations observed in the SC state of several strong type-II superconductors, we have carried out μSR and superconducting quantum interference device (SQUID) magnetization measurements on the borocarbides discussed above, and compared them with dHvA measurements on similar borocarbide samples. Such comparative measurements enable us to trace possible correlations between the local (μSR) and global (SQUID) magnetization changes in the sample with changes in dHvA amplitude.

The measurements show that phase smearing is much too small to account for the enhanced additional damping. It is also found that strong disorder of the vortex lattice, revealed by characteristic change of the μSR line shape, is correlated with the strong suppression of the dHvA signal in the PE region, whereas the establishment of a well-ordered vortex lattice well below the PE region closely follows the weak additional damping of the dHvA signal, observed in this broad field range. Both findings strongly support a scenario whereby quasiparticle scattering is enhanced by the disorder of the vortex lattice. It should be stressed here that nothing specific to the borocarbides is inherent to this interpretation,

so one expects it to be applicable to other strong type-II superconductors in the PE region, as well.

II. EXPERIMENT

High-quality single crystals of $\text{LuNi}_2\text{B}_2\text{C}$ [$H_{c2}(0) \approx 7$ T] and $\text{YNi}_2\text{B}_2\text{C}$ [$H_{c2}(0) \approx 6$ T] were prepared by the flux-growth technique at Ames Laboratory, USA,¹⁴ and by the zone-melting method at the IFW Dresden, Germany,¹⁵ respectively. The SQUID magnetization measurements were performed at the Dresden High Magnetic Field Laboratory, Germany, while the μSR experiments were carried out at TRIUMF, Vancouver, Canada. The dHvA data exploited in the comparative analysis were extracted from previous measurements employing the field-modulation technique on $\text{LuNi}_2\text{B}_2\text{C}$ at $T = 0.5$ K.⁷ A detailed discussion of their dHvA signal in the normal state and the electronic band structure is given in Ref. 16. Note that, due to technical reasons, the μSR measurements were carried out on samples similar but not identical to the ones where the dHvA effect was measured. Furthermore, it is not currently feasible to carry out μSR measurements below 2 K in fields above 5 T. Thus, in order to allow cross correlation between magnetization and μSR measurements, the magnetization was also measured using a SQUID magnetometer on the same samples and at the same temperatures as employed in the μSR experiments.

Transverse-field (TF) μSR measurements up to 7 T were carried out on the M15 muon beam line at TRIUMF using the HiTime spectrometer, which consists of muon and positron detectors contained within a standard He-flow cryostat. The external field was directed parallel to the c axis of each crystal. A fast Fourier transform (FFT) of the TF- μSR signal closely resembles the internal magnetic-field distribution $P(B)$.¹⁷ The measurements were typically done by cooling the sample in a fixed field to a temperature between 2 and 3 K, and then measuring the field dependence of the TF- μSR signal. Specifically, measurements were performed on the $\text{LuNi}_2\text{B}_2\text{C}$ single crystal after field cooling in 3 and 7 T, and on $\text{YNi}_2\text{B}_2\text{C}$ after field cooling in 0.5 and 3 T. Several temperature-dependent measurements were also made. In addition, measurements were performed on each sample above T_c at 20 K to visualize the broadening of the TF- μSR line shape by nuclear moments and the field inhomogeneity of the external magnet.

III. RESULTS

A typical result from a series of systematic dHvA measurements on the flux-grown $\text{LuNi}_2\text{B}_2\text{C}$ crystal is shown in Fig. 1 for various fields parallel to the c axis. A similar result for slightly different field orientation was reported in Ref. 7 (see, e.g., Fig. 7 there). The drop seen in the Dingle plot of the dHvA signal (originating from the spherical Fermi surface¹⁶) just below the SC transition is nicely correlated with the PE seen in the magnetization envelope. This feature and the weak additional attenuation of the dHvA signal seen below the PE region essentially agree with the results reported for $\text{YNi}_2\text{B}_2\text{C}$ in Refs. 4 and 6. One should note that the extraction of the dHvA signal at the PE region is somewhat ambiguous since a reliable determination of the large nonoscillating PE background signal is challenging. The background signal was

subtracted by fitting suitable polynomials to the raw-data signal. Specifically, polynomials of orders between 3 and 5, and in field ranges between two and five magnetic oscillations, were examined in the fitting process. The resulting error in the dHvA amplitude, about 15%, is sufficiently smaller than the average reduction of amplitude observed in the PE region ($\sim 50\%$) to justify our conclusion that the damping of the dHvA oscillation observed in the PE region is significantly stronger than in its immediate vicinity. Above and below the PE, the error was found to be much lower than 5%. The Dingle data were generated from the background-subtracted signal using step-by-step Fourier transforms over three oscillations.

Results of our μ SR measurements are shown in Fig. 2. The upper panel in Fig. 2 shows FFTs of the measured μ SR signals for $\text{LuNi}_2\text{B}_2\text{C}$, after field cooling to 2.3 K in 3 T, and the

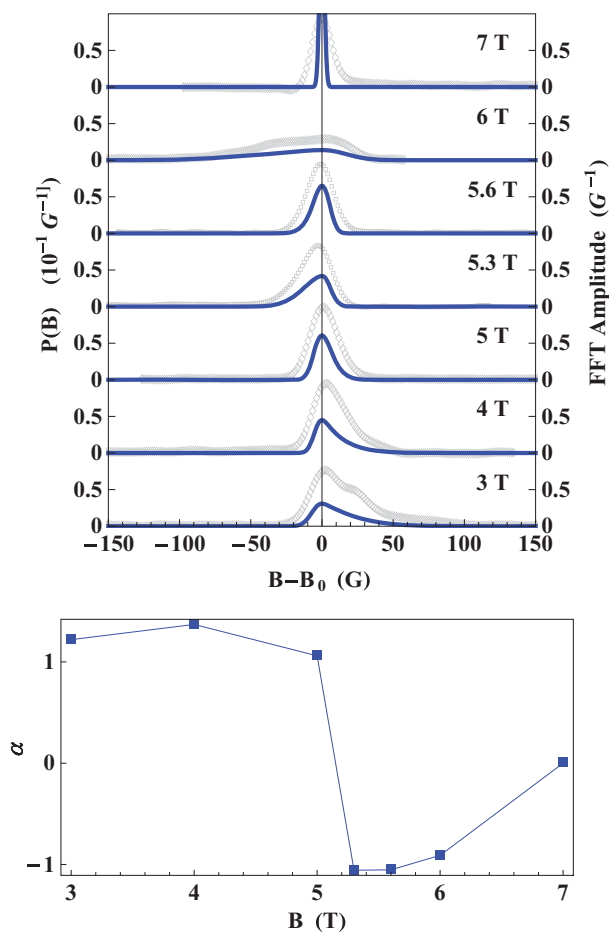


FIG. 2. (Color online) (Upper panel) Probability field-distribution lines $P(B)$, for $\text{LuNi}_2\text{B}_2\text{C}$ (solid lines) at different external magnetic fields, derived by deconvoluting the FFTs (open symbols) of the μ SR signals. Measurements at $H = 3, 4, 5$, and 6 T were done after field cooling to 2.3 K at 3 T, whereas at $H = 5.3$ and 5.6 T were performed after degaussing at 2.7 K. The lines were displaced vertically for clarity and horizontally for comparison. The reference data used in the deconvolution were measured on the same sample above T_c at $T = 20$ K. The shoulder seen on the 3-T FFT curve around 25 G is due to muons that missed the SC sample. (Lower panel) Field dependence of the skewness parameter α (see text) as calculated from the field distributions shown in the upper panel. The line connecting the data points is a guide to the eyes.

corresponding probability field distribution $P(B)$ obtained by deconvoluting each FFT curve with respect to the (practically Gaussian) reference signal. The onset of a large broadening of $P(B)$ and its reversed skewness in a small field range around 6 T are apparent. The dramatic skewness reversal of the line shape is illustrated in the lower panel of Fig. 2, where the skewness parameter $\alpha = \langle \Delta B^3 \rangle^{1/3} / (\langle \Delta B^2 \rangle^{1/2})$, with $\Delta B = B - \langle B \rangle$ (Ref. 17), is plotted for the various distribution functions.

One should be aware of the kinetic nature of the PE, which is reflected by the history dependence of the measured μ SR data. For example, field cooling in 3 T followed by an increase in field to 6 T results in a line shape with a negative α (see Fig. 2), whereas field cooling in 7 T followed by a reduction of the field to 6 T results in a positive α (not shown). However, for this specific cooldown path, negative skewness was found for the 6.5 -T measurement. One may also note the small bumpy change of the field distribution width between 5 and 5.3 T in Fig. 3, which seems to result from the different field histories of the measurements. The overall picture of negative skewness in the PE region, however, is clearly established.

It has been shown in Ref. 18 that a negative α is due to the presence of short-range triplet correlation in the absence of long-range order, characterizing a vortex glass phase. Thus, the onset of negative α (around 5 T in Fig. 2) just below the PE region (Fig. 3) indicates that the vortex lattice is disordered in the entire PE region. Remarkably, the sharp change of α is seen to correlate with the appearance of the PE and the additional damping of the dHvA oscillation shown in Fig. 1. Note that changes in the skewness parameter stretch over a larger field range (see Fig. 3) than the line broadening. This may be due to the fact that large broadening follows the onset of the vortex glass state, whereas strong disorder characterizes both the vortex liquid and glass states. The important point is that they both change significantly in the PE region.

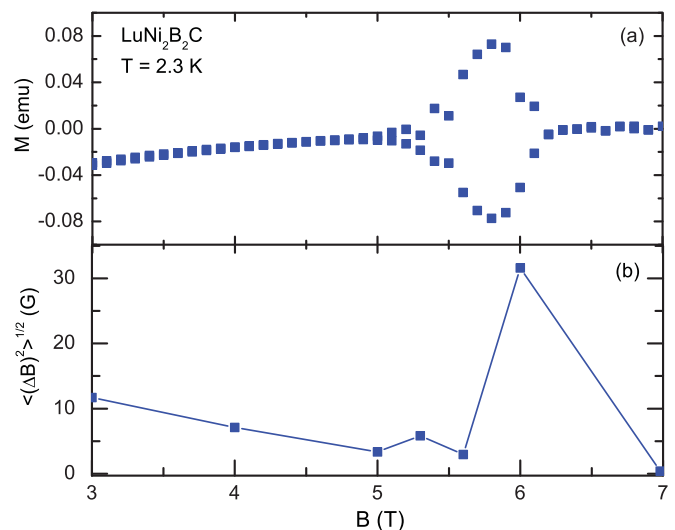


FIG. 3. (Color online) Field dependence of the longitudinal magnetic moment $\text{LuNi}_2\text{B}_2\text{C}$ around the PE region obtained by SQUID magnetization measurements at $T = 2.3$ K (upper panel), and the corresponding field dependence of the μ SR field distribution width (lower panel) calculated from the data shown in Fig. 2. The line connecting the data points is a guide to the eyes.

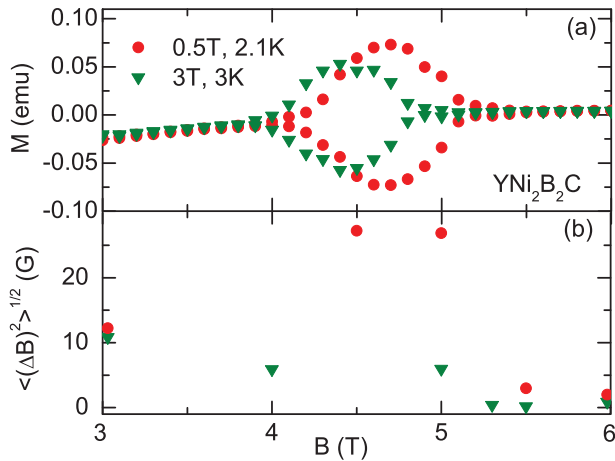


FIG. 4. (Color online) (a) Field dependence of the longitudinal magnetic moment of $\text{YNi}_2\text{B}_2\text{C}$ near the PE region obtained by SQUID magnetization measurements for the indicated cooldown conditions at 2.1 and 3 K. (b) Field dependence of the μSR field distribution width calculated from the data obtained at 2.1 and 3 K.

The positive values of α near unity in a broad field range below the PE reflect the occurrence of a well-ordered vortex lattice in this region, which is seen to correlate with the weak additional damping of the dHvA signal.

Finally, our isothermal SQUID magnetization measurements, performed on both $\text{LuNi}_2\text{B}_2\text{C}$ and $\text{YNi}_2\text{B}_2\text{C}$ samples, are shown in Figs. 3 and 4, respectively. The magnetization data around the PE regions are plotted together with the width of the TF- μSR lines. The sharp maximum in the μSR linewidth, shown for both $\text{LuNi}_2\text{B}_2\text{C}$ (Fig. 3) and $\text{YNi}_2\text{B}_2\text{C}$ (Fig. 4), closely follows the PE in the corresponding magnetization curve. It should be noted, however, that the magnitude and field range of the PE depend on temperature. As shown in Figs. 4 and 5, lowering the temperature shifts the PE in the SQUID magnetization to higher fields and increases its width. Thus, we conclude that the difference between the TF- μSR linewidths observed after field cooling in 0.5 T to 2.1 K and after field cooling in 3 T to 3 K, are primarily due to a thermal effect. This effect accounts for the relative shift

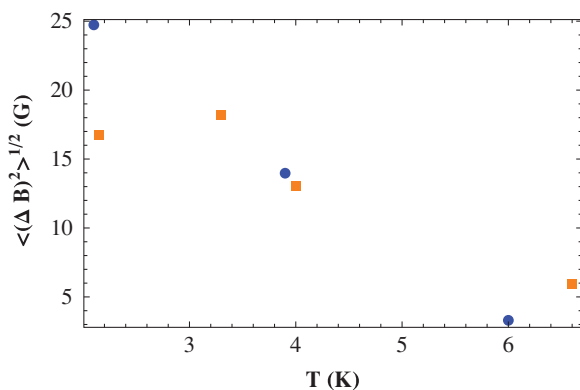


FIG. 5. (Color online) Temperature dependence of the field distribution width, measured after 3 T (squares) and 0.5 T (circles) cooldowns. For each cooldown, the measurements were done at a certain field, i.e., 4.5 T for the 0.5 T cooldown and 3 T for the 3 T cooldown.

between the PE position shown in Fig. 1 and that shown in Fig. 3. However, as clearly seen in Fig. 5, the field distribution width does not exceed an upper bound of 25 G at 2.1 K, which is not expected to significantly increase at lower temperatures, where the system is below the disordered vortex phase.¹⁹

IV. DISCUSSION

Summarizing our experimental results, significant line broadening and reversed skewness have been observed in μSR measurements, both correlated with the observation of a PE and an enhanced damping of the dHvA oscillations. The origin of this remarkable correlation is most probably due to enhanced pinning-induced vortex-lattice disorder. However, the enhanced field inhomogeneity observed in the PE region, approximately 40 G (maximal field distribution width in the PE) in both $\text{LuNi}_2\text{B}_2\text{C}$ and $\text{YNi}_2\text{B}_2\text{C}$ (Figs. 3 and 4), seems to be too small to attribute the additional damping of the dHvA amplitude to further broadening of the Landau levels by magnetic-field inhomogeneity.

The following analysis establishes this conclusion: Imagine a charged quasiparticle (with an effective mass m^*) moving freely in a two-dimensional spatial field profile $B(\mathbf{r})$, consisting of a large uniform part B_0 plus a small nonuniform part $B_1(\mathbf{r}) \equiv B(\mathbf{r}) - B_0$. The distribution of $B_1(\mathbf{r})$ is assumed to be completely random, so its ensemble average is $\langle B_1(\mathbf{r}) \rangle = 0$. The Landau-level width π/τ_R at the Fermi energy E_F , corresponding to the unperturbed cyclotron frequency $\omega_c = eB_0/m^*c$ due to the inhomogeneous broadening, is given in the semiclassical limit $n_F = E_F/\hbar\omega_c \gg 1$, by²⁰ $\frac{\pi}{\tau_R\omega_c} = (\frac{m^*E_F}{\hbar^2})^{1/2} \frac{\sqrt{\langle b^2 \rangle}}{B_0}$, where $\langle b^2 \rangle = \int \langle B_1(\mathbf{r})B_1(\mathbf{r}') \rangle d^2r'$. For a random vortex distribution near H_{c2} , the correlation length is of the order of the minimal (magnetic) length $a_{B_0} \equiv \sqrt{c\hbar/eB_0}$ and $\langle b^2 \rangle \simeq B_1^2 a_{B_0}^2$, with $B_1^2 = \langle B_1^2(\mathbf{r}) \rangle$, so that

$$\frac{\pi}{\tau_R\omega_c} = n_F^{1/2} \left(\frac{B_1}{B_0} \right). \quad (1)$$

The damping of the dHvA amplitude associated with the Landau-level broadening described above can be estimated from the Dingle factor $R_D = \exp(-\frac{\pi}{\tau_R\omega_c})$. This may be compared with the extra damping factor due to direct scattering of a quasiparticle by the pair potential in the random vortex distribution limit,^{1,12} which takes the form

$$R_M = \exp\left(-\frac{\pi}{\tau_M\omega_c}\right), \quad \frac{\pi}{\tau_M\omega_c} = \pi^{3/2} \frac{\widetilde{\Delta}_0^2}{n_F^{1/2}}, \quad (2)$$

where $\widetilde{\Delta}_0 \equiv \Delta_0/\hbar\omega_c$, and Δ_0 is the self-consistent Ginzburg-Landau expression for the amplitude of the SC order parameter. At the PE field position $B = B_{PE} \lesssim H_{c2}$, i.e., $B_{PE} \simeq 6$ T, with $H_{c2} \simeq 7$ T (at about 3 K), we find $\widetilde{\Delta}_0^2 \approx 0.36n_F(1 - B_{PE}/H_{c2})$, so that combining Eq. (1) with Eq. (2) one has

$$\frac{\tau_M}{\tau_R} \simeq \frac{1}{2(1 - B_{PE}/H_{c2})} \left(\frac{B_1}{H_{c2}} \right) = 3 \times 10^{-3}. \quad (3)$$

Here we take $B_1 = 40$ G as an upper bound to the measured field distribution width, as shown in Fig. 3.

The Dingle plot obtained from Eq. (2), modified by thermal fluctuations⁶ for reasonable values of the adjustable parameters

Δ_0 and H_{c2} ,⁷ is shown in Fig. 1 to agree well with the experimental Dingle plot in the PE region. Thus, Eq. (3) implies that the additional damping rate associated with the enhanced field inhomogeneity observed in the PE region is at least two orders of magnitude smaller than the observed damping rate shown in Fig. 1.

The above estimate indicates that, in order to reasonably account for the striking drop observed in the dHvA amplitude at the PE region, one should invoke the direct influence of the SC pair potential on the fermionic quasiparticles under quantizing magnetic field, rather than the indirect effect through the magnetic-field inhomogeneity induced by the SC currents. Within this interpretation, the observed recovery of the dHvA signal below the PE region, shown in Fig. 1, is

explained by the reduced additional damping of the dHvA amplitude in the Abrikosov vortex lattice^{1,11} as compared to that predicted for the random vortex distribution.¹

ACKNOWLEDGMENTS

This research was supported by the Israel Science Foundation Grant No. 425/07, by Posnansky Research fund in superconductivity, and by EuroMagNET under EU contract No. 228043. J. E. Sonier acknowledges support from the Natural Sciences and Engineering Research Council of Canada. Work at the Ames Laboratory was supported by the Department of Energy, Basic Energy Sciences, under Contract No. DE-AC02-07CH11358.

*maniv@tx.technion.ac.il

¹T. Maniv, V. Zhuravlev, I. D. Vagner, and P. Wyder, *Rev. Mod. Phys.* **73**, 867 (2001).

²C. Jaudet *et al.*, *Phys. Rev. Lett.* **100**, 187005 (2008).

³T. J. B. M. Janssen, C. Haworth, S. M. Hayden, P. Meeson, M. Springford, and A. Wasserman, *Phys. Rev. B* **57**, 11698 (1998).

⁴T. Terashima, C. Haworth, H. Takeya, S. Uji, H. Aoki, and K. Kadowaki, *Phys. Rev. B* **56**, 5120 (1997).

⁵T. Isshiki, N. Kimura, H. Aoki, T. Terashima, S. Uji, K. Yamauchi, H. Harima, D. Jaiswal-Nagar, S. Ramakrishnan, and A. K. Grover, *Phys. Rev. B* **78**, 134528 (2008).

⁶T. Maniv, V. Zhuravlev, J. Wosnitza, O. Ignatchik, B. Bergk, and P. C. Canfield, *Phys. Rev. B* **73**, 134521 (2006).

⁷B. Bergk and J. Wosnitza, *Low Temp. Phys.* **35**, 687 (2009).

⁸R. Corcoran, N. Harrison, S. M. Hayden, P. Meeson, M. Springford, and P. J. van der Wel, *Phys. Rev. Lett.* **72**, 701 (1994).

⁹S. Dukan and Z. Tesanovic, *Phys. Rev. B* **49**, 13017 (1994); *Phys. Rev. Lett.* **74**, 2311 (1995).

¹⁰M. R. Norman, A. H. MacDonald, and H. Akera, *Phys. Rev. B* **51**, 5927 (1995); M. R. Norman and A. H. MacDonald, *ibid.* **54**, 4239 (1996).

¹¹K. Yasui and T. Kita, *Phys. Rev. B* **66**, 184516 (2002).

¹²K. Maki, *Phys. Rev. B* **44**, 2861 (1991).

¹³M. J. Stephen, *Phys. Rev. B* **45**, 5481 (1992).

¹⁴P. C. Canfield, P. L. Gammel, and D. J. Bishop, *Phys. Today* **51**, 40 (1998).

¹⁵G. Behr *et al.*, *J. Cryst. Growth* **198/199**, 642 (1999).

¹⁶B. Bergk, V. Petzold, H. Rosner, S.-L. Drechsler, M. Bartkowiak, O. Ignatchik, A. D. Bianchi, I. Sheikin, P. C. Canfield, and J. Wosnitza, *Phys. Rev. Lett.* **100**, 257004 (2008).

¹⁷J. E. Sonier, J. H. Brewer, and R. F. Kiefl, *Rev. Mod. Phys.* **724**, 769 (2000).

¹⁸G. I. Menon *et al.*, *Phys. Rev. Lett.* **97**, 177004 (2006).

¹⁹D. Jaiswal-Nagar, D. Pal, M. R. Eskildsen, P. C. P. Canfield, H. Takeya, S. Ramakrishnan, and A. K. Grover, *Pramana* **66**, 113 (2006).

²⁰A. G. Aronov, E. Altshuler, A. D. Mirlin, and P. Wolfe, *Europhys. Lett.* **29**, 239 (1995).